UNIVERSITY
OF TRENTO

DIPARTIMENTO DI INGEGNERIA E SCIENZA DELL'INFORMAZIONE

38123 Povo – Trento (Italy), Via Sommarive 14
http://www.disi.unitn.it

ADAPTIVENULLING IN TIME-MODULATED LINEAR ARRAYS WITHMINIMUM POWER LOSSES

L. Poli, P. Rocca, G. Oliveri, and A. Massa

January 2011

Technical Report # DISI-11-102

Adaptive Nulling in Time-Modulated Linear Arrays with Minimum Power Losses

L. Poli, P. Rocca, G. Oliveri, and A. Massa

Department of Information Engineering and Computer Science,

University of Trento, Via Sommarive 14, 38123 Trento - Italy

Tel. +39 0461 882057, Fax +39 0461 882093

E-mail: *andrea.massa@ing.unitn.it*,

{*lorenzo.poli*, *paolo.rocca*, *giacomo.oliveri*}*@disi.unitn.it*

Web-site: *http://www.eledia.ing.unitn.it*

Adaptive Nulling in Time-Modulated Linear Arrays with Minimum Power Losses

L. Poli, P. Rocca, G. Oliveri, and A. Massa

Abstract

The synthesis of adaptive time-modulated linear arrays is dealt with by means of an innovative strategy, in which a Particle Swarm Optimizer is used to reconfigure the pulse sequence controlling the static element excitations, as well as the least significant bits of digital phase shifters to maximize the signal-to-interference-plus-noise ratio at the receiver. The reduction of the power content of sideband radiation generated by the periodic on-off commutation of switches is addressed by customizing to non-isotropic sources a very effective analytic relationship. A set of selected results is reported and discussed to show the advantages and limitations of the proposed approach. Comparisons with previously published results are also presented.

Key words: Adaptive Nulling, Time-Modulated Linear Arrays, Sideband Radiation, Particle Swarm Optimization.

1 Introduction

Adaptive antenna arrays are key devices for many applications in radars and communications [1] because of the need to properly receive a desired signal in the presence of interferences or jammers. Dealing with adaptive phased-arrays, several techniques have been proposed to control the element weights for synthesizing beam pattern nulls along the directions of arrival (DoAs) of the undesired signals [2]-[5]. For hardware (HW) architectures with a receiver at each array element, amplitude and phase weights can be efficiently reconfigured by multiplying the quiescent coefficients by the inverse of the covariance matrix [2]. Although very effective, such a solution has not been adopted widely because of the HW complexity and the high costs. Commercial arrays generally have only one output whose value is equal to the sum of the power of the signals impinging on the antenna array. Furthermore, phase-only adaptive strategies are usually preferred to the use of tunable amplitude weights [3]-[5] due to the cheap costs and the reliability of digital phase shifters. Therefore, binary optimization strategies based on evolutionary algorithms have been used. Genetic Algorithms (GAs) have been used in [6] to set the least significant bits of the digital phase shifters for minimizing the total output power. It has been proved that small variations of the phase weights provide very effective nulling results in different scenarios, while small changes of the position of the main beam guarantee a suitable reception of the desired signal. Following this, learning strategies exploiting the memory on the control history have been integrated in GA-based approaches [7][8] to increase the time-reaction of the system. More recently, the Particle Swarm Optimizer (PSO) has addressed pattern nulling problems [9], outperforming other adaptive algorithms. A memory-enhanced version has been investigated also in this case to face more complex scenarios characterized by jammers located in both the far-field and the near-field of the receiving antenna [10].

In recent years, time-modulated arrays have attracted growing interest since they overcome some classical drawbacks of the amplitude-weight control by arbitrarily shaping the radiated pattern by means of the modulation of the static excitations [11]-[18] with a set of radio-frequency (RF) switches. However, in this case the main disadvantage is the generation of unwanted harmonic radiations. To address these issues, an approach based on a Hybrid Differential Evolution (HDE) algorithm has been developed for time-modulated linear geometries

(i.e., time-modulated linear arrays - $TMLA$s) [19]. The minimization of the total output power has been carried out as in [6], but here the optimization of the least significant bits of the digital phase shifters as well as the pulse sequence controlling the static excitations have been optimized. Thanks to the exploitation of the additional degrees of freedom (in the time domain), not considered in [6], deeper nulls have been obtained in the directions of the undesired signals. The sideband level (SBL), namely the peak level of the sideband radiations (SRs), has also been minimized, yielding satisfactory results [19]. However, such a SBL optimization to compensate the SR losses presents two drawbacks. First, it does not usually consider the total amount of power losses in harmonic radiations since the evaluation of the SBL is generally limited to the first harmonic patterns [11][12][19]. Second, the evaluation of the SBL is cumbersome from a computational point of view, since the generation of the whole set of harmonic patterns is required.

As an alternative to the above, we present an innovative PSO-based adaptive nulling strategy based on the maximization of the signal-to-interference-plus-noise ratio. To deal with the SR optimization, the analytical relationship derived in [20], which allows an exact computation of the contribution of the infinite harmonic radiations, has been modified to encompass the use of non-isotropic sources, as well. The PSO has been used to optimize the pulse sequence controlling the static excitations as well as the least significant bits of the digital phase shifters, whose weights have been supposed with an odd-symmetrical distribution to achieve the nulling with minimum perturbation of their phase values [21].

The rest of the paper is organized as follows. The problem is mathematically formulated in Section 2, where the adaptive nulling strategy is also described. The results of a set of numerical experiments are reported and discussed in Section 3 to point out advantages and limitations of the proposed approach (Section 3.1) as well as for comparisons with state-of-the-art methods (Section 3.2). Finally, conclusions are given in Section 4.

2 Mathematical Formulation

Let us consider a time-modulated linear array composed of N point sources with $\sin\theta$ element patterns (i.e., collinear short dipoles) equally-spaced along the z-axis. A desired signal and I

interferences impinge on the antenna from θ_d and θ_i, $i = 1, ..., I$, different directions, respectively. The electromagnetic signals are assumed to be narrow-band plane waves with central angular frequency $\omega_0 = 2\pi f_0$. The antenna output when at least one element is time-modulated is given by [22]

$$F(t, \theta) = e^{j\omega_0 t} \sin\theta \sum_{n=1}^{N} \alpha_n U_n(t) e^{j\beta\left[n-\left(\frac{N+1}{2}\right)\right]d\cos\theta} \tag{1}$$

where $\alpha_n = A_n e^{j\varphi_n}$, $n = 1, ..., N$, is the n-th complex static excitation, A_n and φ_n being the corresponding amplitude weight and phase weight, respectively. Moreover, d is the inter-element distance and $\beta = \frac{\omega_0}{c}$ is the free-space wavenumber, c being the speed of light in vacuum. Furthermore, $U_n(t) = U_n(t + kT_p)$, $h \in \mathbb{Z}$, is a periodic rectangular pulse function of period T_p that models the on-off behaviour of an RF switch used to modulate the n-th array element where

$$U_n(t) = \begin{cases} 1 & 0 < t \leq \tau_n T_p \\ 0 & t > \tau_n T_p \end{cases} \tag{2}$$

$\tau_n \in [0,\, 1]$ being the normalized duration of the "on" state of the n-th element (the so-called *switch-on time*). By considering the Fourier expansion of the modulating pulses, $U_n(t) = \sum_{h\in\mathbb{Z}} u_{nh} e^{jh\omega_p t}$, $n = 1, ..., N$, $u_{nh} = \frac{1}{T_p}\int_0^{T_p} U_n(t)\, e^{-jh\omega_p t} dt$ being the Fourier coefficient and $\omega_p = \frac{2\pi}{T_p}$, Equation (1) can be expressed as the summation of infinite harmonic terms spaced by ω_p [22]. More specifically, the term at the central frequency ($h = 0$) turns out to be

$$F_0(\theta) = \sin\theta \sum_{n=1}^{N} \alpha_n \tau_n e^{j\beta\left[n-\left(\frac{N+1}{2}\right)\right]d\cos\theta} \tag{3}$$

where $\tau_n = u_{n0}$, $n = 1, ..., N$, while the SR contribution is equal to [20]

$$F_{SR}(\theta, t) = \sum_{h\in\mathbb{Z},\, h\neq 0} e^{jh\omega_p t} \sin\theta \sum_{n=1}^{N} \alpha_n u_{nh} e^{j\beta\left[n-\left(\frac{N+1}{2}\right)\right]d\cos\theta}. \tag{4}$$

The power at the array elements from the desired signal is

$$\Upsilon_d = \left| \sin\theta_d s_d \sum_{n=1}^{N} \alpha_n \tau_n e^{j\beta\left[n-\left(\frac{N+1}{2}\right)\right]d\cos\theta_d} \right|^2 \tag{5}$$

where s_d is the received signal strength, while the amount of undesired power collected by the receiver is $\Upsilon_u = \Upsilon_i + \Upsilon_n$ where

$$\Upsilon_i = \left| \sum_{i=1}^{I} \sin\theta_i s_i \sum_{n=1}^{N} \alpha_n \tau_n e^{j\beta\left[n-\left(\frac{N+1}{2}\right)\right]d\cos\theta_i} \right|^2 \tag{6}$$

is related to the I interfering signals, s_i, $i = 1, ..., I$, being the strength of the i-th signal, and Υ_n is the power of the noise modeled as an AWG process.

To maximize the signal-to-interference-plus-noise ratio ($SINR$), the problem at hand is formulated as in [7][9] and the following functional is maximized

$$\Psi^{SINR}\left(\underline{\tau}, \underline{\varphi}\right) = \frac{\Upsilon_d\left(\underline{\tau}, \underline{\varphi}\right)}{\Upsilon_d\left(\underline{\tau}, \underline{\varphi}\right) + \Upsilon_u\left(\underline{\tau}, \underline{\varphi}\right)} \tag{7}$$

to determine the two sets of unknowns $\underline{\tau} = \{\tau_n,\ n = 1, ..., N\}$ and $\underline{\varphi} = \{\varphi_n,\ n = 1, ..., N\}$. Dealing with time-modulation, Equation (7) is properly integrated with a suitable additive term to take into account the power losses due to the modulation of the static excitations

$$\Psi_{SR}^{SINR}\left(\underline{\tau}, \underline{\varphi}\right) = \Psi^{SINR}\left(\underline{\tau}, \underline{\varphi}\right) + \frac{P_0\left(\underline{\tau}, \underline{\varphi}\right)}{P_{tot}\left(\underline{\tau}, \underline{\varphi}\right)} \tag{8}$$

where $P_0\left(\underline{\tau}, \underline{\varphi}\right) = P_{tot}\left(\underline{\tau}, \underline{\varphi}\right) - P_{SR}\left(\underline{\tau}, \underline{\varphi}\right)$ is the power associated to the pattern at the central frequency, P_{tot} and P_{SR} being the total power and the losses in the SR, respectively. This latter quantity is computed using the analytical relationship in [20] evaluated for point sources

$$P_{SR} = \frac{4}{3}\sum_{n=1}^{N}\left\{|\alpha_n|^2\tau_n\left(1-\tau_n\right)\right\} + 2 \sum_{\substack{m,n=1 \\ m\neq n}}^{N} \left\{ \mathrm{Re}\left(\alpha_m\alpha_n^*\right)\left[\frac{\mathrm{sinc}\left(\xi\right)-\cos\left(\xi\right)}{\xi^2}\right]\left(\hat{\tau}-\tau_m\tau_n\right)\right\} \tag{9}$$

where $\xi = \beta d\left(m-n\right)$ and $\hat{\tau} = \tau_n$ if $\tau_n \leq \tau_m$ and $\hat{\tau} = \tau_m$, otherwise. Moreover, $\mathrm{Re}\left(\cdot\right)$ and $*$ denote the real part and complex conjugation, respectively.

The optimization of (7) or (8) is carried out by means of the inertial weight version of the PSO algorithm [23] following the guidelines described in [9] and extended to the synthesis of time-modulated arrays in [24].

3 Numerical Results

In this section, a set of numerical experiments is reported and discussed to assess the effectiveness of the proposed adaptive nulling strategy. Whatever test case, if it is not specified, the electromagnetic source of the desired signal is assumed to be in broadside (i.e., $\theta_d = 90^o$) with power $\Upsilon_d = 0\,dB$ and the environment is modelled with a level of noise $30\,dB$ below the strength of the desired signal ($\Upsilon_n = -30\,dB$). As far as the PSO is concerned, a swarm of $S = 2 \times N$ particles has been used in all the experiments and the control parameters have been set according to the indications given in [25]. Both cognitive (C_1) and social (C_2) acceleration coefficients have been fixed to 2, while the inertial weight (ω) has been linearly decreased throughout the iterative optimization from 0.9 to 0.4.

The first two numerical experiments are aimed at showing the effectiveness of the $SINR$-based approach for adaptive nulling, never considered before (to the best of the authors' knowledge) for the synthesis of time-modulated arrays. Towards this aim, isotropic sources have been considered instead of small dipoles [i.e., in (1) and in the formulation the term $sin\theta$ has been set equal to one as in [24]] to show the behaviour of the proposed method without any bias related to the kind of radiating sources. Accordingly, in the first experiment, a single interference ($I = 1$) of power $\Upsilon_1 = 30dB$ impinges on a linear array of $N = 20$ equally-spaced elements ($d = 0.5\lambda_0$, λ_0 being the wavelength at the central frequency) from $\theta_1 = 158^o$. The static array configuration is characterized by real weight coefficients with uniform amplitudes ($A_n = 1$, $n = 1, ..., N$) and null phases ($\varphi_n = 0$, $n = 1, ..., N$). By optimizing $\underline{\tau}$, the pulse sequences and the corresponding radiation patterns at ω_0 and $(\omega_0 + h\omega_p)$, $h = 1, 2$ synthesized with the PSO are displayed in Fig. 1. More specifically, Figures 1(*a*)-(*b*) are concerned with the maximization of the unconstrained $SINR$ functional (7), while the results of the joint optimization of the $SINR$ and of the sideband power losses are reported in Figs. 1(*c*)-(*d*). As expected, since both sets α_n, $n = 1, ..., N$, and τ_n, $n = 1, ..., N$, are real, the pattern $F_0(\theta)$ turns out to be symmetric. For completeness, the behaviour of the cost function that corresponds to the optimal solution of the swarm during the iterative process is given in Fig. 2.

As can be observed, the null is correctly placed along the direction of the interferer in both cases (Fig. 1) and the null depth turns out to be $71\,dB$ and $90\,dB$, respectively (Fig. 3). The

advantages derived from the P_{SR} minimization are non-negligible. On the one hand, the total amount of power losses in the SR reduces from 5.86% down to 1.34% of the radiated power. Moreover, a significant reduction of the SBL has also been achieved (e.g., almost $13\,dB$ for $h = 1$ since $SBL = -23.6\,dB$ goes down to $SBL^{SR} = -36.4\,dB$) as seen in the plots in Fig. 4, where the sideband level of the first 20 harmonic patterns, $SBL^{(h)}$, $h = 1, ..., 20$, are reported. On the other hand, only one switch is required to generate the pulse configuration in Fig. 1(*c*) and the 16-th element is turned-off, while 18 switches are necessary when the SR term is not taken into account during the optimization. As a final remark, while the sidelobe level (SLL) of the pattern at the central frequency is slightly improved (although not involved in the optimization) from $SLL = -13.6\,dB$ to $SLL^{SR} = -14.4\,dB$, it is worth pointing out that the antenna directivity also increases because of the reduction of the power losses. It turns out that $D_{max}^{SR} = 12.7\,dB$ against $D_{max} = 11.1\,dB$[(1)].

The second experiment deals with a multiple-jamming configuration. Three interferences with equal power ($\Upsilon_i = 30dB$, $i = 1, 2, 3$) impinge on the antenna from $\theta_1 = 4^o$, $\theta_2 = 130^o$, and $\theta_3 = 173^o$. The solutions synthesized at the end of the optimization processes are given in Fig. 5. Also in this case, the undesired signals are efficiently suppressed and three nulls (Fig. 6) are located at the convergence in correspondence with the DoAs of the jammers. As expected, similar conclusions to those from the previous example arise by comparing the solutions with and without the SR constraining term in the cost function to be maximized. The power losses are halved ($P_{SR}^{(SINR)} = 6.58\%$ vs. $P_{SR}^{(SINR-SR)} = 2.75\%$) and the maximum directivity increases by almost $1dB$ from $D_{max} = 11.7\,dB$ up to $D_{max}^{SR} = 12.6\,dB$. Moreover, the $SBL^{(h)}$ values turn out to be always smaller that those without the SR constraint (Fig. 7). As regards the HW architecture, fewer than half the switches (i.e., 4 against 9) are required to modulate the array according to the pulse sequence of Fig. 5(*c*) instead of using the configuration in Fig. 5(*a*).

Since adaptive nulling in $TMLA$s has been already dealt with in the literature, the results of some comparisons with the solutions achieved in [19] where the nulling has been obtained through the minimization of the total output power with the HDE-based approach are shown and discussed in the following. For fair comparisons, short dipoles are considered and the

(1) The directivity values have been computed by exploiting the relationship available in [26].

unknowns to be optimized are now the time durations, $\underline{\tau}$, and the phase coefficients, $\underline{\varphi}$. As in [19], the phase shifters are characterized by $B = 6$ bits and only the two least significant ($L = 2$) have been modified during the optimization process. However, unlike [19], anti-symmetric phases have been considered on the one hand to take into account the same number of degrees of freedom in the synthesis process and on the other hand to fully exploit the suggestion in [6][21] about nulling efficiency of phase distribution[(2)]. As for the switch-on times, the admissible perturbations have been limited to $\pm 0.23 T_p$ (i.e., $\tau_n \in [\tau_n^{init} \pm 0.23]$, $n = 1, ..., N$, τ_n^{init} being the n-th guess switch-on-time).

The first comparison considers a $TMLA$ of $N = 40$ elements ($d = 0.5\lambda_0$) and two interferers from $u_1 = \cos\theta_1 = 0.62$ (i.e., $\theta_1 = 51.68^o$) and $u_2 = \cos\theta_2 = 0.72$ (i.e., $\theta_2 = 43.95^o$) both with power $60\,dB$ over the desired signal ($\Upsilon_i = 60\,dB$, $i = 1, 2$). The starting pulse sequence has been set to afford a Dolph-Chebyshev pattern [28] at ω_0 with $SLL = -30dB$ (i.e., $\tau_n^{init} = \tau_n^{DC}$, $n = 1, ..., N$) and uniform static excitations have been chosen ($A_n = 1$, $n = 1, ..., N$) to simplify the architecture of the beam forming network, as well.

The HDE, aimed at reducing the SR losses through the SBL minimization, required 250 iterations (Fig. 8) to place nulls of $\left|\frac{F_0(\theta_i)}{max\{F_0(\theta)\}}\right|^2 \simeq -50\,dB$ at the interference DoAs (even though $\left|\frac{F_0(\theta_i)}{max\{F_0(\theta)\}}\right|^2 + \Upsilon_i \simeq 10\,dB$, $i = 1, 2$) with $SBL^{HDE} = max_h \left\{SBL^{HDE(h)}\right\}$ equal to $-16.7\,dB$ [19]. In contrast, the proposed PSO-based approach has yielded null depths of $-160\,dB$, far below the levels reached with the HDE, just after 200 iterations (Fig. 8) by computing the SR using (9) throughout the optimization process. The pulse sequence and the phase weights at the PSO convergence are shown in Fig. 9, while the radiated patterns at the central frequency and at $\omega_0 + h\omega_p$, $h = 1, 2$, are reported in Fig. 10. As it can be observed (Fig. 10), the maximum value of SBL has been lowered of more than $3\,dB$ ($SBL^{PSO}_{SINR-SR} = -20.2\,dB$), as well. However, the SLL of the PSO solution turns out to be higher than the HDE one [19] ($SLL^{PSO}_{SINR-SR} = -16.0\,dB$ vs. $SLL^{HDE} = -27.0\,dB$). This is not surprising because of the even distribution about the centre of the HDE phases used to keep low the SLL of the radiation at ω_0 [6][27]. To also address the SLL minimization with odd phase shifts, a suitable forcing term has been added to (8)

(2) *"Lowering the sidelobe levels requires an even phase shift about the center of the array [27], while nulling requires an odd phase shift* [21]" [6].

$$\Psi_{SR-SLL}^{SINR}\left(\underline{\tau},\underline{\varphi}\right)=\Psi_{SR}^{SINR}\left(\underline{\tau},\underline{\varphi}\right)+\frac{\left|SLL\left(\underline{\tau},\underline{\varphi}\right)\right|}{\left|SLL^{ref}\right|} \tag{10}$$

where $SLL \triangleq \max_{\theta\in\Theta_{\rm SLL}}\left\{\frac{F_0(\theta)}{\max_{0\leq\phi\leq\pi}[{\rm F}_0(\phi)]}\right\}$ and Θ_{SLL} identifies the range of angular directions outside the main beam region. Following such a strategy and setting $SLL^{ref}=-30\,dB$, the patterns shown in Fig. 11 have been synthesized. The jammers are still efficiently suppressed with nulls deeper than $-100\,dB$, but now the level of the secondary lobes at ω_0 is of the same order of magnitude as the HDE solution (i.e., $SLL_{SINR-SR-SLL}^{PSO}=-24.8\,dB$) with a reduction of more than $8\,dB$ compared to $SBL_{SINR-SR}^{PSO}$. For completeness, the PSO pulse sequence and the phase weights are reported in Fig. 12(*a*) and Fig. 12(*b*), respectively.

The last experiment is concerned with a larger array with $N=100$ elements and $d=0.5\lambda_0$. As in [19], the performances of the PSO adaptive nulling strategy are evaluated when an interfering signal of power $\Upsilon_1=54\,dB$ impinges on the array close to the main lobe ($\theta_1=88.28^o$), while the second one ($\Upsilon_2=46\,dB$) is generated by a source at $\theta_2=43.11^o$. For comparison purposes, $L=4$ bits among the available 6 have been changed as in [19] since placing nulls close to the main beam is expected to need more significant perturbations of the phase weights. Figure 13 shows the patterns synthesized when optimizing (10) by constraining the switch-on times within $\tau_n\in[\tau_n^{init}\pm 0.23]$, $n=1,...,N$, as in [19] [Fig. 13(*a*)] and without constraints on the switching sequence [Fig. 13(*b*)]. In both cases, the jammers are suitably counteracted with null depths lower than $-80\,dB$. As for the other pattern features, the synthesized pattern is characterized by $SLL_{constr}^{PSO}=-14.5\,dB$ in the constrained case ($SLL^{HDE}=-17.5\,dB$) and the SBL is lowered of more than $20dB$ with respect to the HDE solution ($SBL^{HDE}=-20.0\,dB$ vs. $SBL_{constr}^{PSO}=-40.5\,dB$). As expected, the unconstrained solution [Fig. 13(*b*)] also improves the sidelobe level (i.e., $SLL_{unconst}^{PSO}=-18.1\,dB$).

4 Conclusions

In this paper, an innovative strategy for the synthesis of adaptive $TMLA$s has been presented. The complexity of the amplitude control for pattern nulling has been avoided by optimizing the on-off sequence that modulates the static excitations and the least significant bits of digital

phase shifters by means of a PSO-based approach. To deal with the optimization of the power losses, the standard $SINR$ cost function has been integrated with a computationally-efficient analytical expression customized to take into account also non-isotropic radiators having $\sin\theta$ element pattern. Suitable countermeasures for dealing with the SLL minimization also with anti-symmetric phase distributions of the array elements have also been adopted. A selected set of numerical results as well as representative comparisons with state-of-the-art techniques have been presented and discussed to point out the effectiveness and reliability of the proposed approach which seems to represent a useful tool for communication and radar devices.

References

[1] R. T. Compton, *Adaptive Antennas: Concepts and Performance*. Englewood Cliffs, NJ: Prentice-Hall, 1988.

[2] S. P. Applebaum, "Adaptive arrays," *IEEE Trans. Antennas Propag.*, vol. 24, no. 5, pp. 585-598, Sep. 1976.

[3] C. A. Baird and G. G. Rassweiler, "Adaptive sidelobe nulling using digitally controlled phase-shifters," *IEEE Trans. Antennas Propag.*, vol. 24, pp. 638-649, Sep. 1976.

[4] M. K. Leavitt, "A phase adaptation algorithm," *IEEE Trans. Antennas Propag.*, vol. 24, pp. 754-756, Sep. 1976.

[5] H. Steyskal, "Simple method for pattern nulling by phase perturbation," *IEEE Trans. Antennas Propag.*, vol. 31, pp. 163-166, Jan. 1983.

[6] R. L. Haupt, "Phase-only adaptive nulling with a genetic algorithm," *IEEE Trans. Antennas Propag.*, vol. 45, pp. 1009-1015, Jun. 1997.

[7] D. S. Weile and E. Michielssen, "The control of adaptive antenna arrays with genetic algorithms using dominance and diploidy," *IEEE Trans. Antennas Propag.*, vol. 49, pp. 1424-1433, Oct. 2001.

[8] C. Sacchi, F. De Natale, M. Donelli, A. Lommi, and A. Massa, "Adaptive antenna array control in the presence of interfering signals with stochastic arrivals: assessment of a GA-based procedure," *IEEE Trans. Wireless Commun.*, vol. 3, pp. 1031-1036, Jul. 2004.

[9] M. Donelli, R. Azaro, F. G.B. De Natale, and A. Massa, "An innovative computational approach based on a particle swarm strategy for adaptive phased-arrays control," *IEEE Trans. Antennas Propag.*, vol. 54, pp. 889-898, Mar. 2006.

[10] M. Benedetti, R. Azaro, and A. Massa, "Memory enhanced PSO-based optimization approach for smart antennas control in complex interference scenarios," *IEEE Trans. Antennas Propag.*, vol. 56, pp. 1939-1947, Jul. 2008.

[11] S. Yang, Y. B. Gan, and A. Qing, "Sideband suppression in time-modulated linear arrays by the differential evolution algorithm," *IEEE Antennas Wireless Propag. Lett.*, vol. 1, pp. 173-175, 2002.

[12] S. Yang, Y. B. Gan, and P. K. Tan, "A new technique for power-pattern synthesis in time-modulated linear arrays," *IEEE Antennas Wireless Propag. Lett.*, vol. 2, pp. 285-287, 2003.

[13] J. Fondevila, J. C. Brégains, F. Ares, and E. Moreno, "Optimizing uniformly excited linear arrays through time modulation," *IEEE Antennas Wireless Propag. Lett.*, vol. 3, pp. 298-301, 2004.

[14] S. Yang, Y. B.Gan, A. Qing, and P. K. Tan, "Design of a uniform amplitude time modulated linear array with optimized time sequences," *IEEE Trans. Antennas Propag.*, vol. 53, pp. 2337-2339, Jul. 2005.

[15] J. Fondevila, J. C. Brégains, F. Ares, and E. Moreno, "Application of time modulation in the synthesis of sum and difference patterns by using linear arrays," *Microw. Opt. Technol. Lett.*, vol. 48, pp. 829-832, May 2006.

[16] S. Yang, Z. Nie, and F. Yang, "Synthesis of low sidelobe planar antenna arrays with time modulation," in *Proc. APMC 2005 Asia-Pacific Microw. Conf.*, Suzhou, China, 4-7 Dec. 2005.

[17] Y. Chen, S. Yang, Z. Nie, "Synthesis of satellite footprint patterns from time-modulated planar arrays with very low dynamic range ratios," *Int. J. Numer. Model.*, vol. 21, pp. 493-506, 2008.

[18] L. Manica, P. Rocca, L. Poli, and A. Massa, "Almost time-independent performance in time-modulated linear arrays," *IEEE Antennas Wireless Propag. Lett.*, vol. 8, pp. 843-846, 2009.

[19] Y. Chen, S. Yang, G. Li, and Z. Nie, "Adaptive nulling in time-modulated antenna arrays," *Proc. 2008 8th Int. Symp. Antennas, Propag. & EM Theory (ISAPE 2008)*, Kunming, China, 2-5 Nov. 2008, pp. 713-716.

[20] J. C. Brégains, J. Fondevila, G. Franceschetti, and F. Ares, "Signal radiation and power losses of time-modulated arrays," *IEEE Trans. Antennas Propag.*, vol. 56, pp. 1799-1804, Jun. 2008.

[21] R. A. Shore, "A proof of the odd-symmetry of the phases for minimum weight perturbation phase-only null synthesis," *IEEE Trans. Antennas Propag.*, vol. 32, pp. 528-530, May 1984.

[22] W. H. Kummer, A. T. Villeneuve, T. S. Fong, and F. G. Terrio, "Ultra-low sidelobes from time-modulated arrays," *IEEE Trans. Antennas Propag.*, vol. 11, pp. 633-639, Jun. 1963.

[23] J. Kennedy, R. C. Eberhart, and Y. Shi, *Swarm Intelligence*. San Francisco, CA: Morgan Kaufmann, 2001.

[24] L. Poli, P. Rocca, L. Manica, and A. Massa, "Handling sideband radiations in time-modulated arrays through particle swarm optimization," *IEEE Trans. Antennas Propag.*, vol. 58, pp. 1408-1411, Apr. 2010.

[25] P. Rocca, M. Benedetti, M. Donelli, D. Franceschini, and A. Massa, "Evolutionary optimization as applied to inverse scattering problems," *Inverse Problems*, vol. 25, 123003, pp. 1-41, doi: 10.1088/0266-5611/25/12/123003, Dec. 2009.

[26] S. Yang, Y. B. Gan, and P. K. Tan, “Evaluation of directivity and gain for time-modulated linear antenna arrays,” *Microw. Opt. Technol. Lett.*, vol. 42, pp. 167-171, Jul. 2004.

[27] J. F. Deford and O. P. Gandhi, “Phase-only synthesis of minimum peak sidelobe patterns for linear and planar arrays,” *IEEE Trans. Antennas Propag.*, vol. 36, pp. 191-201, Jan. 1988.

[28] R. S. Elliott, *Antenna theory and design*. Wiley-Interscience, IEEE Press, 2003.

FIGURE CAPTIONS

- **Figure 1.** *Numerical Validation - Single Interference* ($N = 20$; $I = 1$ - $\theta_1 = 158^o$, $\Upsilon_1 = 30dB$). Plots of the (*a*)(*c*) pulse sequences and of the (*b*)(*d*) normalized power patterns at the central frequency ($h = 0$) and at the harmonic radiations $h = \{1, 2\}$ synthesized by the PSO approach (*a*)(*b*) without [Eq. (7)] and (*c*)(*d*) with SR constraint [Eq. (8)].

- **Figure 2.** *Numerical Validation - Single Interference* ($N = 20$; $I = 1$ - $\theta_1 = 158^o$, $\Upsilon_1 = 30dB$). Behavior of the optimum value of the cost function throughout the iterative PSO-based optimization.

- **Figure 3.** *Numerical Validation - Single Interference* ($N = 20$; $I = 1$ - $\theta_1 = 158^o$, $\Upsilon_1 = 30\,dB$). Behavior of the null depth versus the iteration index k.

- **Figure 4.** *Numerical Validation - Single Interference* ($N = 20$; $I = 1$ - $\theta_1 = 158^o$, $\Upsilon_1 = 30\,dB$) - Plots of the sideband levels $SBL^{(h)}$, $h \in [1,\, 20]$, of the PSO solutions synthesized without [Eq. (7)] and with the SR constraint [Eq. (8)].

- **Figure 5.** *Numerical Validation - Multiple Interferences* ($N = 20$; $I = 3$ - $\theta_1 = 4^o$, $\theta_2 = 130^o$, and $\theta_3 = 173^o$, $\Upsilon_i = 30\,dB$). Plots of the (*a*)(*c*) pulse sequences and of the (*b*)(*d*) normalized power patterns at the central frequency ($h = 0$) and at the harmonic radiations $h = \{1, 2\}$ synthesized by the PSO approach (*a*)(*b*) without [Eq. (7)] and (*c*)(*d*) with SR constraint [Eq. (8)].

- **Figure 6.** *Numerical Validation - Multiple Interferences* ($N = 20$; $I = 3$ - $\theta_1 = 4^o$, $\theta_2 = 130^o$, and $\theta_3 = 173^o$, $\Upsilon_i = 30\,dB$). Behavior of the null depth versus the iteration index k.

- **Figure 7.** *Numerical Validation - Multiple Interferences* ($N = 20$; $I = 3$ - $\theta_1 = 4^o$, $\theta_2 = 130^o$, and $\theta_3 = 173^o$, $\Upsilon_i = 30\,dB$). Plots of the sideband levels $SBL^{(h)}$, $h \in [1,\, 20]$, of the PSO solutions synthesized without [Eq. (7)] and with the SR constraint [Eq. (8)].

- **Figure 8.** *Comparative Assessment - Multiple Interferences* ($N = 40$; $I = 2$ - $\theta_1 =$

51.68^o, $\theta_2 = 43.95^o$, $\Upsilon_i = 60\,dB$). Behaviors of the null depths along the interferer DoAs ($u_1 = \cos\theta_1$, $u_2 = \cos\theta_2$) versus the iteration index k using the PSO approach with SR constraint [Eq. (8)] and the HDE approach [19].

- **Figure 9.** *Comparative Assessment - Multiple Interferences* ($N = 40$; $I = 2$ - $\theta_1 = 51.68^o$, $\theta_2 = 43.95^o$, $\Upsilon_i = 60\,dB$). Plots of the (*a*) pulse sequence and of the (*b*) phase values synthesized by the PSO approach with SR constraint [Eq. (8)].

- **Figure 10.** *Comparative Assessment - Multiple Interferences* ($N = 40$; $I = 2$ - $\theta_1 = 51.68^o$, $\theta_2 = 43.95^o$, $\Upsilon_i = 60\,dB$). Normalized power patterns at the central frequency ($h = 0$) and at the harmonic radiations $h = \{1, 2\}$ synthesized with the PSO approach with SR constraint [Eq. (8)].

- **Figure 11.** *Comparative Assessment - Multiple Interferences* ($N = 40$; $I = 2$ - $\theta_1 = 51.68^o$, $\theta_2 = 43.95^o$, $\Upsilon_i = 60\,dB$). Normalized power patterns at the central frequency ($h = 0$) and at the harmonic radiations $h = \{1, 2\}$ synthesized with the PSO approach with constraints on both SR and SLL [Eq. (10)].

- **Figure 12.** *Comparative Assessment - Multiple Interferences* ($N = 40$; $I = 2$ - $\theta_1 = 51.68^o$, $\theta_2 = 43.95^o$, $\Upsilon_i = 60\,dB$). Plots of the (*a*) pulse sequence and of the (*b*) phase values synthesized by the PSO approach with constraints on both SR and SLL [Eq. (10)].

- **Figure 13.** *Comparative Assessment - Large Array* ($N = 100$; $I = 2$ - $\theta_1 = 43.11^o$, $\Upsilon_1 = 54\,dB$, $\theta_2 = 88.28^o$, $\Upsilon_2 = 46\,dB$) - Plots of the (*a*)(*b*) normalized power patterns at the central frequency ($h = 0$) and at the harmonic radiations $h = \{1, 2\}$, (*c*)(*d*) pulse sequences, and (*e*)(*f*) phase values synthesized by the PSO approach [Eq. (10)] with (*left column*) and without switch-on-time constraints (*right column*).

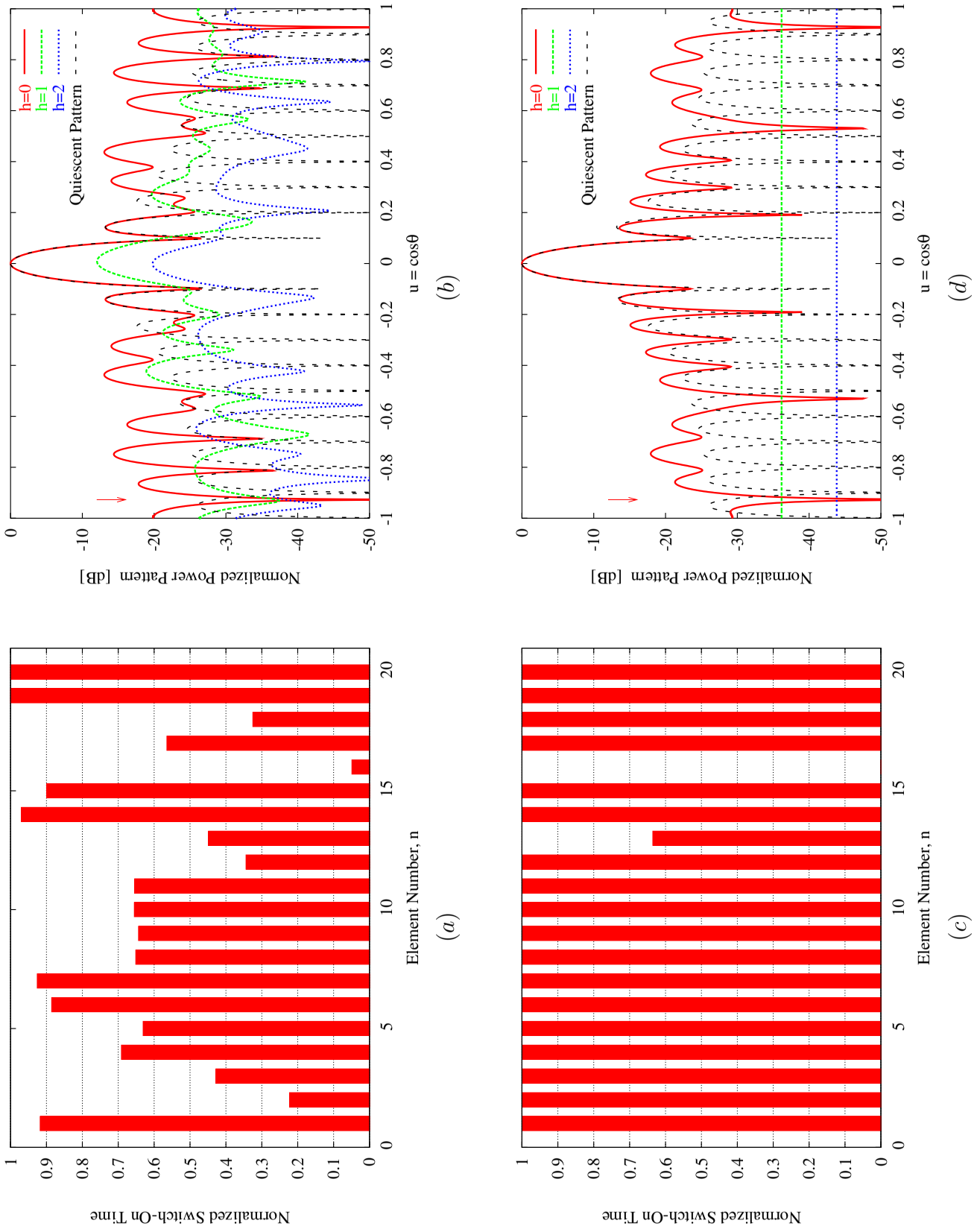

Fig. 1 - L. Poli *et al.*, "Adaptive nulling in time-modulated linear arrays ..."

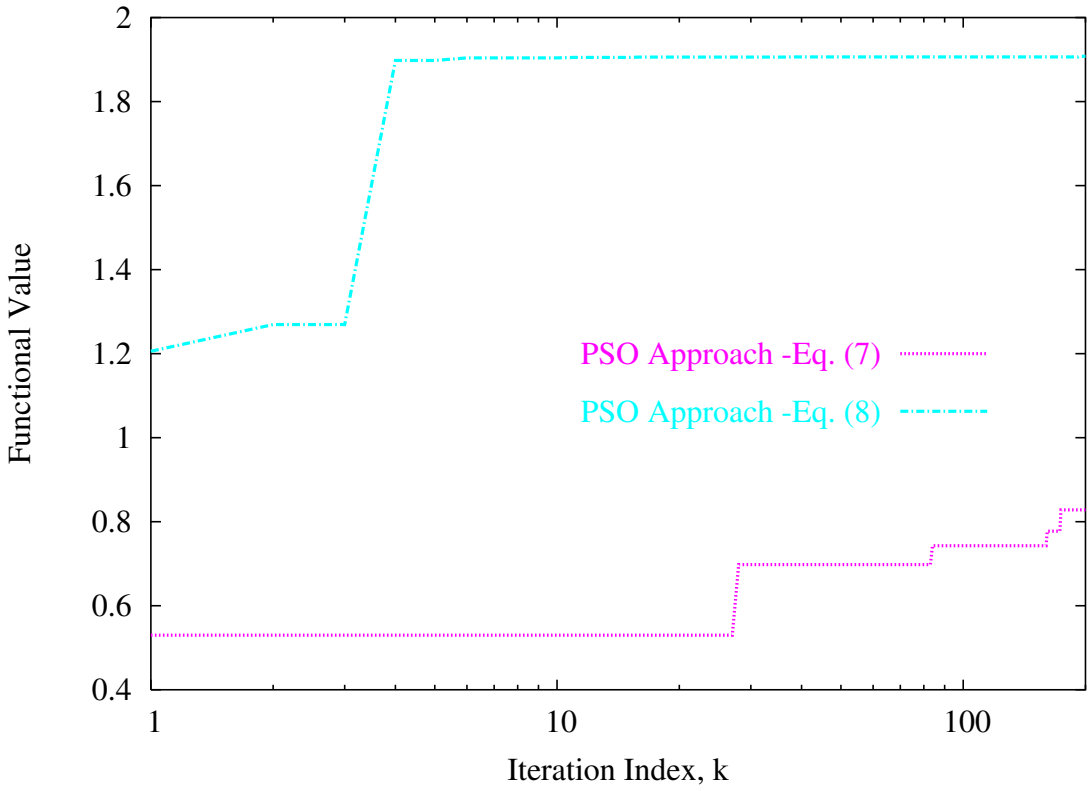

Fig. 2 - L. Poli *et al.,* "Adaptive nulling in time-modulated linear arrays ..."

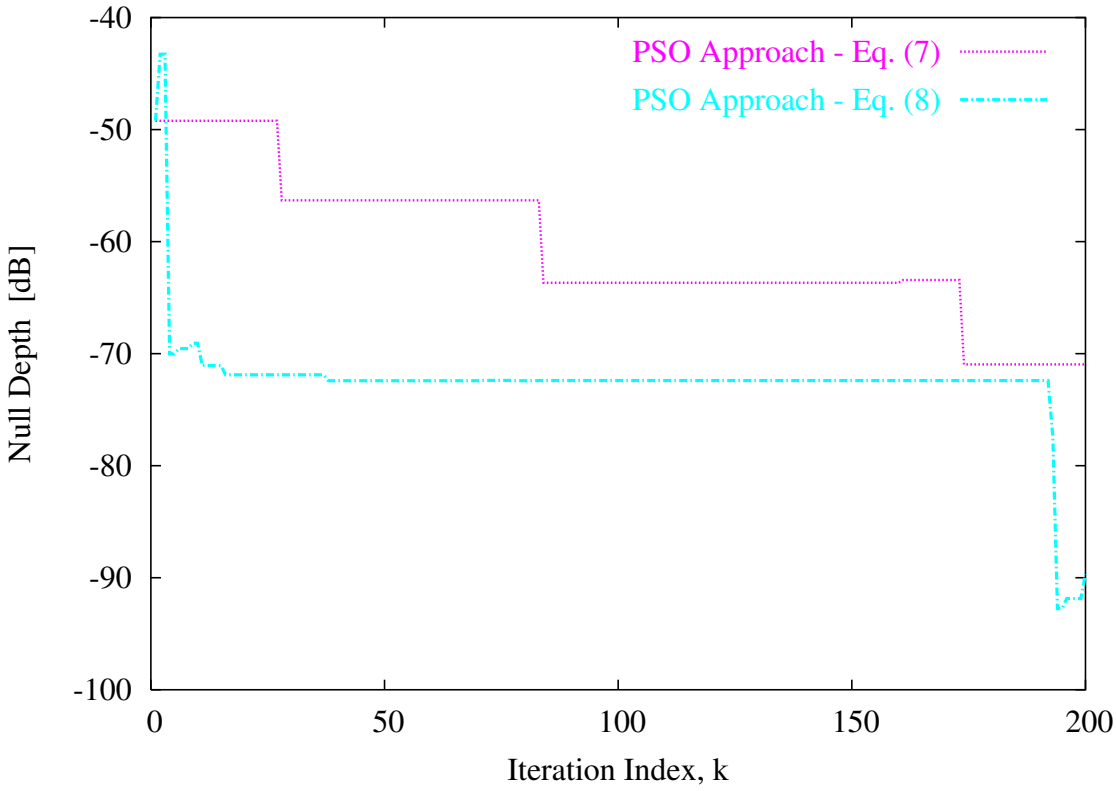

Fig. 3 - L. Poli *et al.,* "Adaptive nulling in time-modulated linear arrays ..."

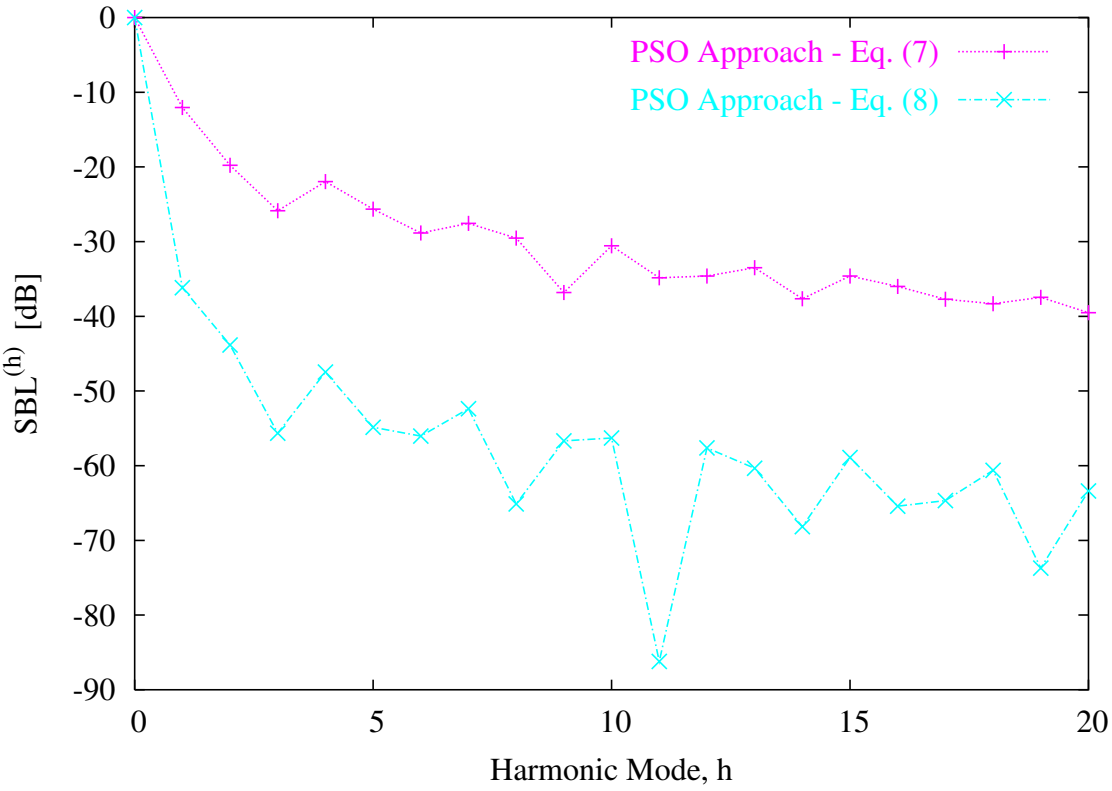

Fig. 4 - L. Poli *et al.,* "Adaptive nulling in time-modulated linear arrays ..."

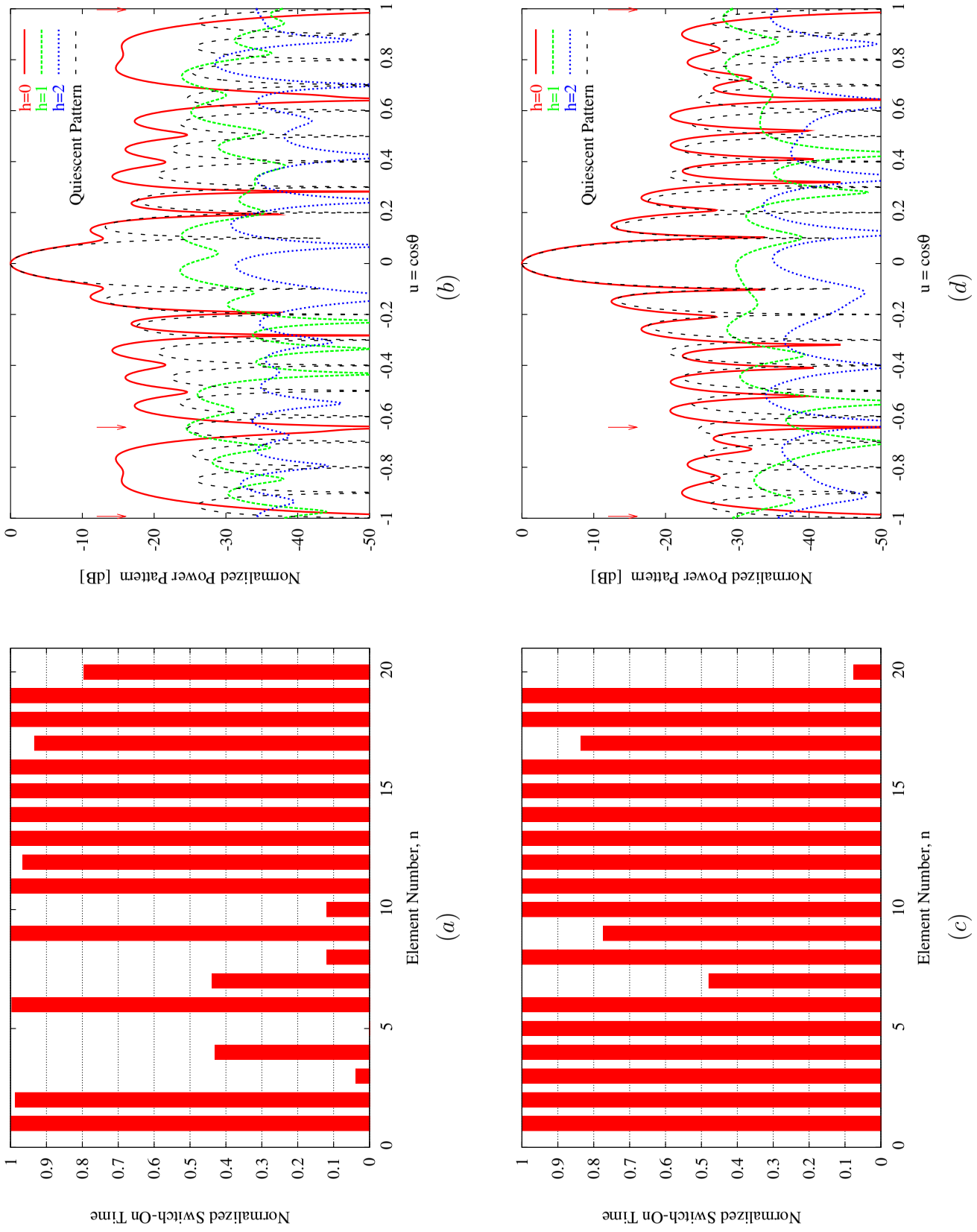

Fig. 5 - L. Poli *et al.*, "Adaptive nulling in time-modulated linear arrays ..."

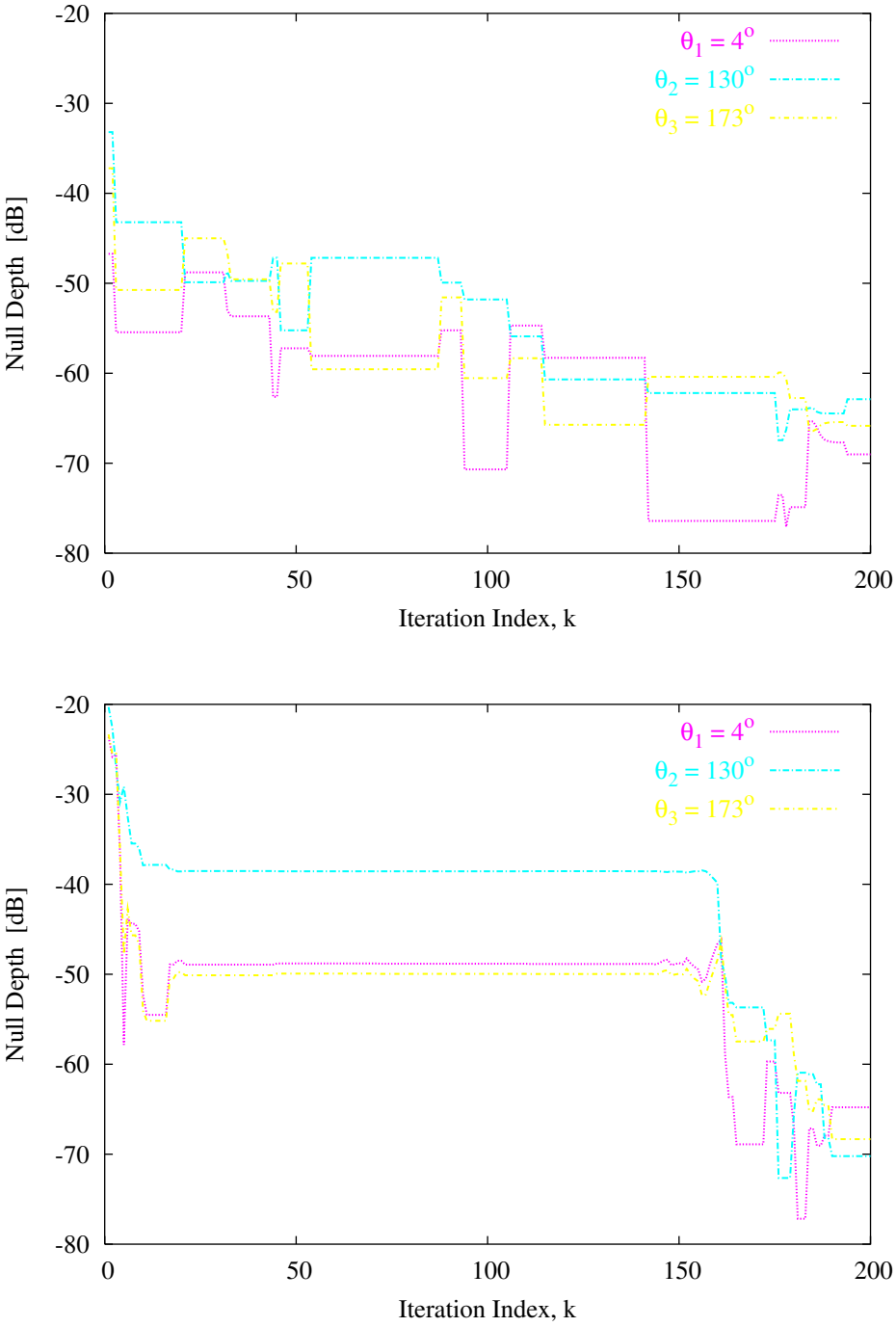

Fig. 6 - L. Poli *et al.,* "Adaptive nulling in time-modulated linear arrays ..."

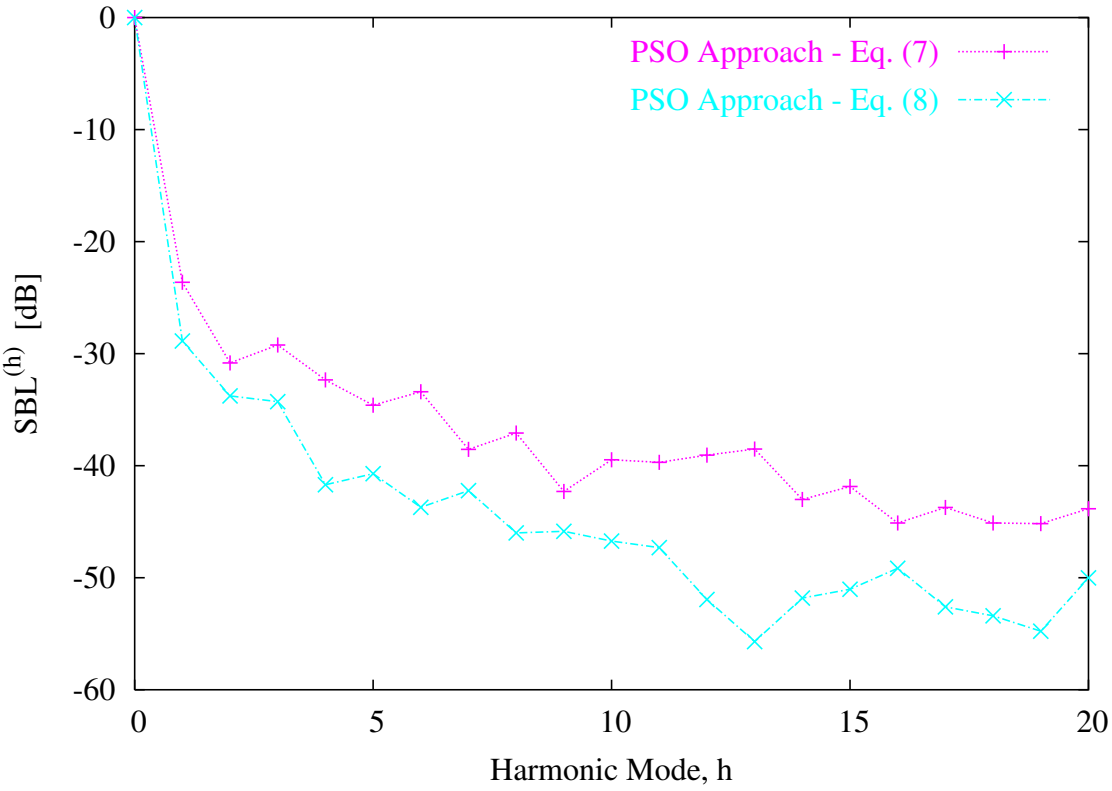

Fig. 7 - L. Poli *et al.,* "Adaptive nulling in time-modulated linear arrays ..."

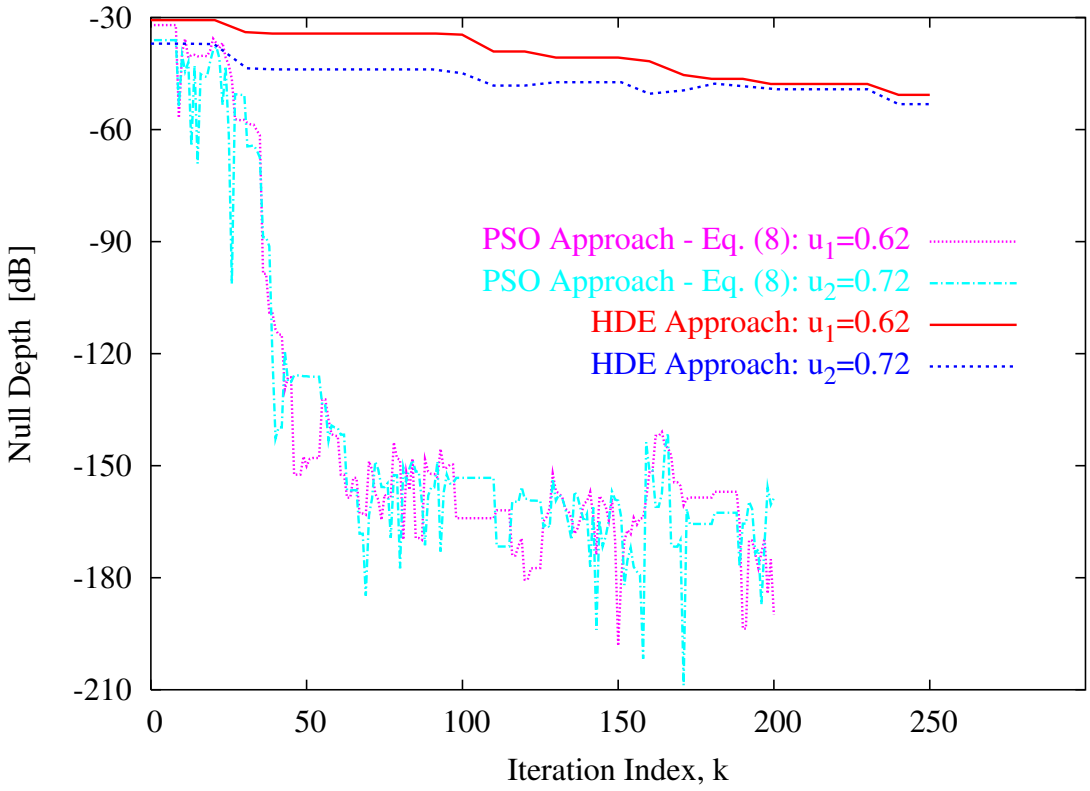

Fig. 8 - L. Poli *et al.,* "Adaptive nulling in time-modulated linear arrays ..."

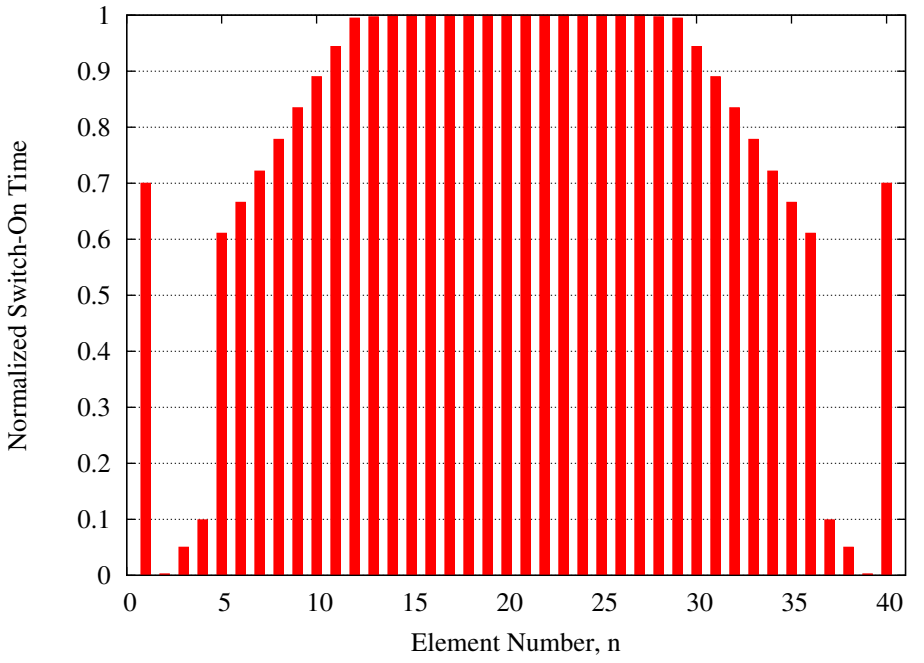

(a)

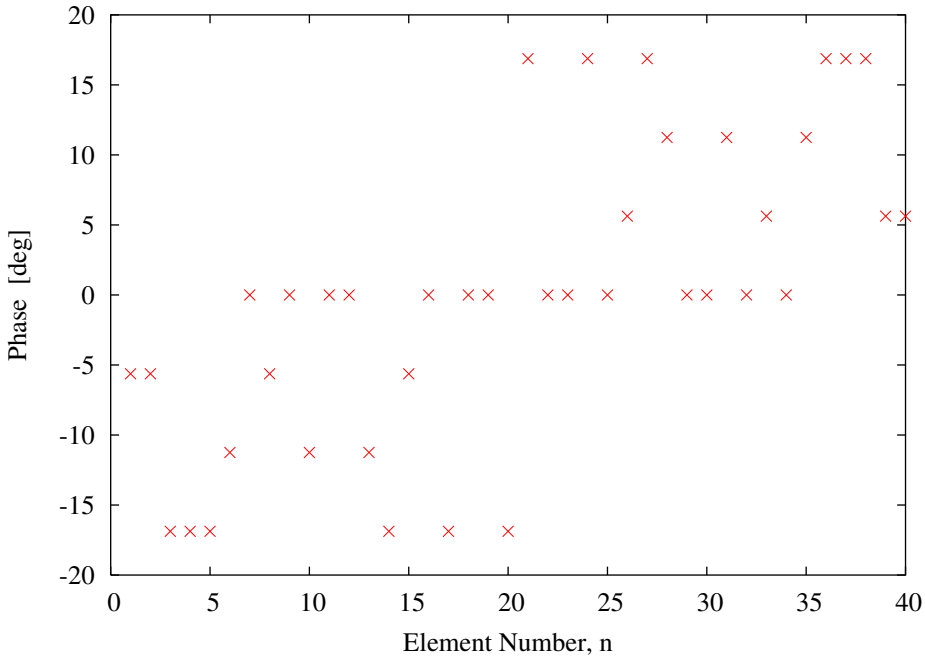

(b)

Fig. 9 - L. Poli *et al.,* "Adaptive nulling in time-modulated linear arrays ..."

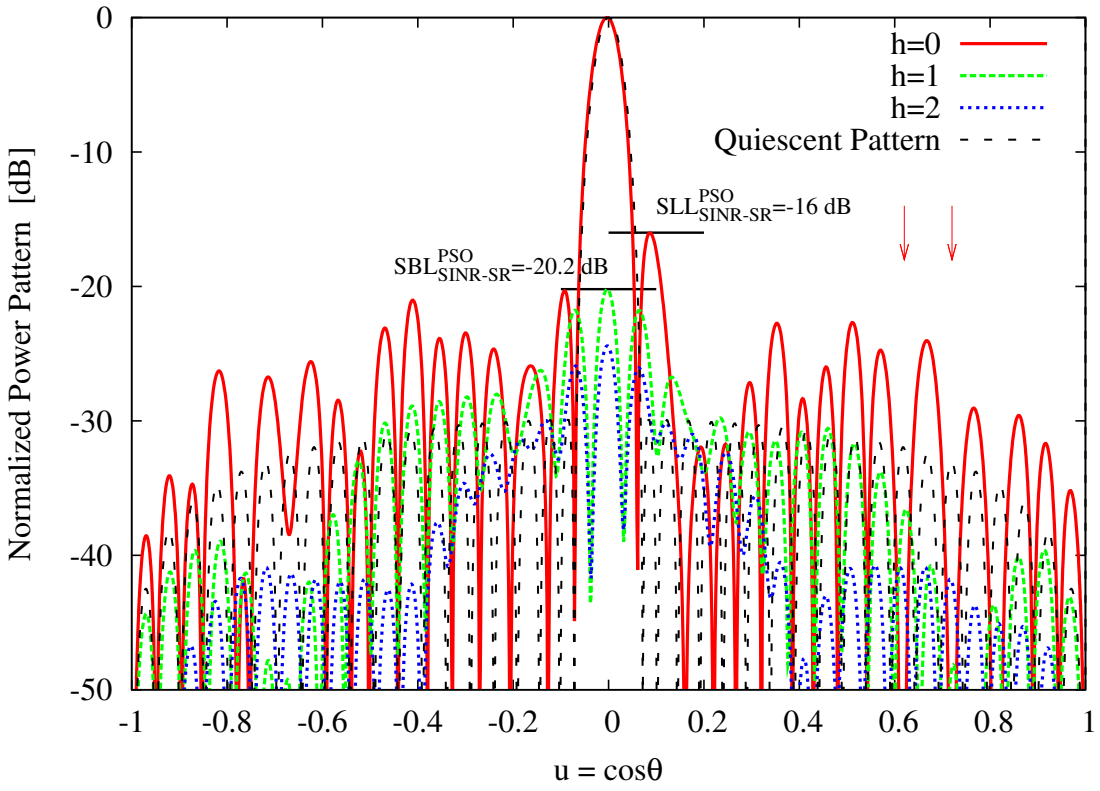

Fig. 10 - L. Poli *et al.*, "Adaptive nulling in time-modulated linear arrays ..."

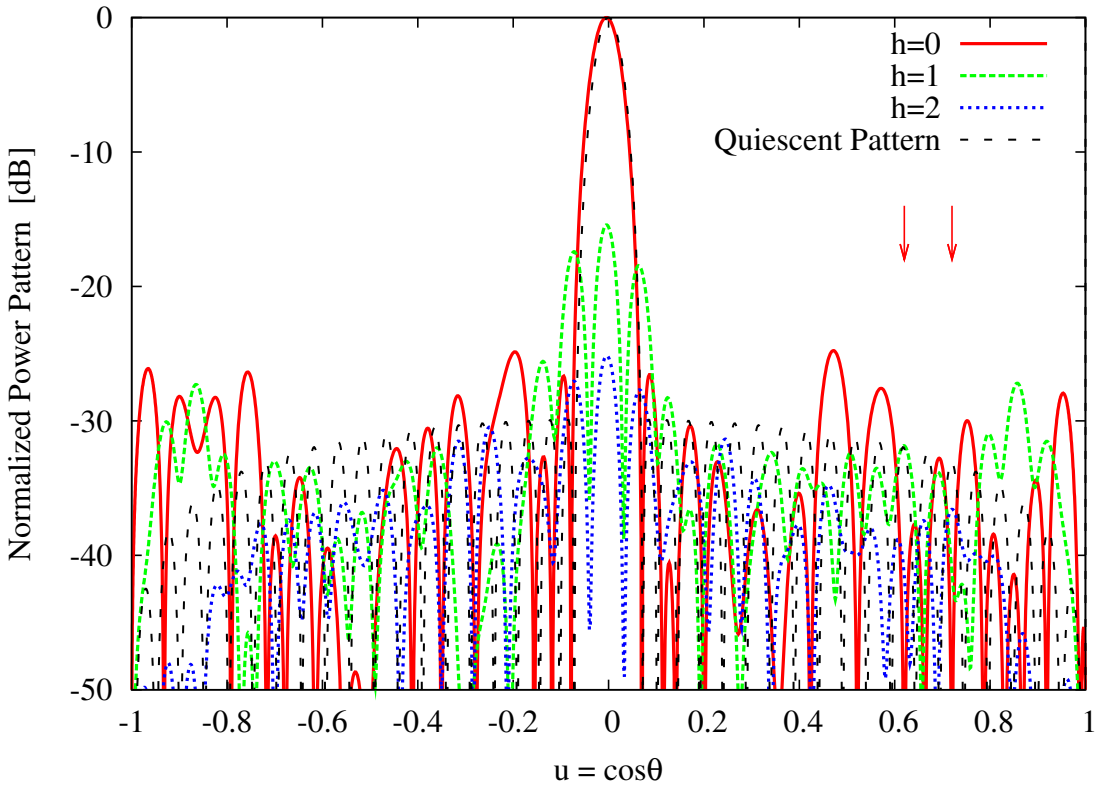

Fig. 11 - L. Poli *et al.*, "Adaptive nulling in time-modulated linear arrays ..."

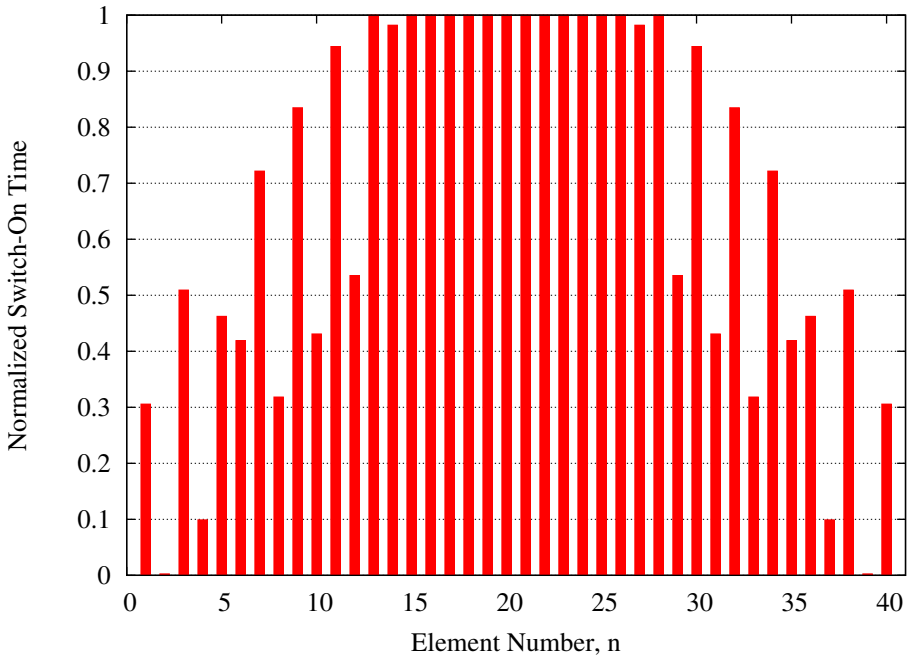

(a)

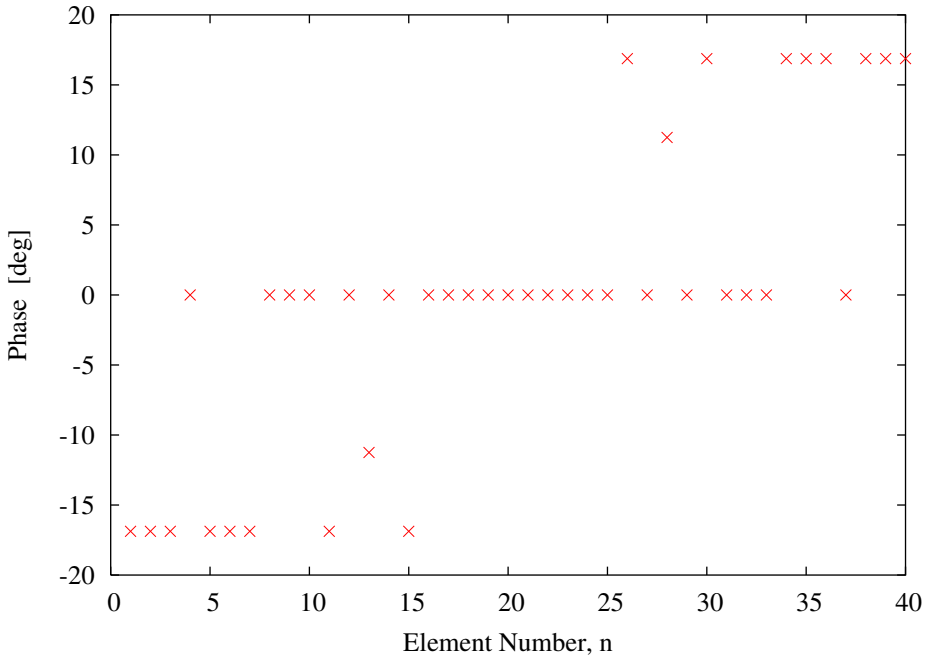

(b)

Fig. 12 - L. Poli *et al.*, "Adaptive nulling in time-modulated linear arrays ..."

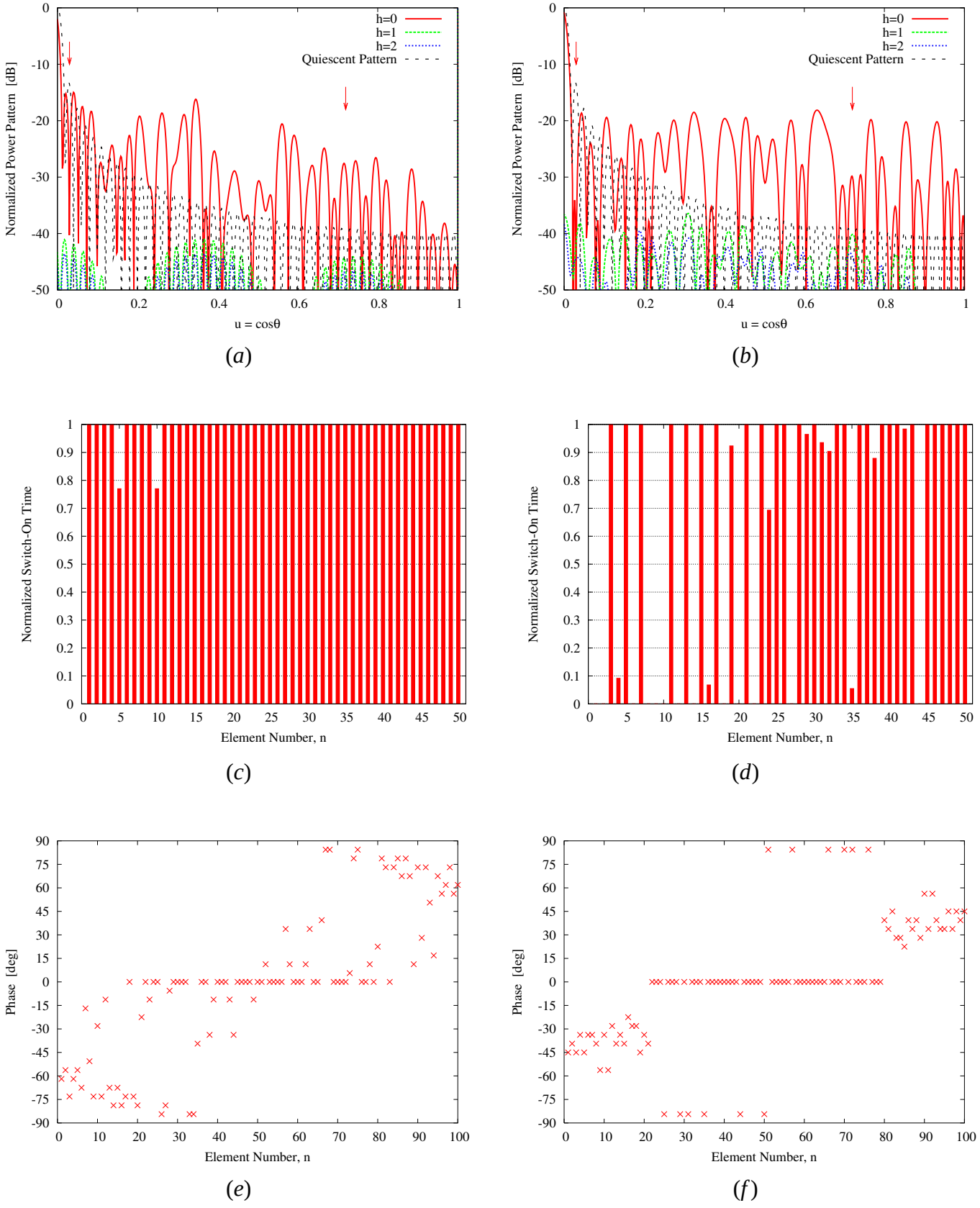

Fig. 13 - L. Poli *et al.*, "Adaptive nulling in time-modulated linear arrays ..."